A Versatile Bistatic & Polarimetric Marine Radar Simulator

Andreas Arnold-Bos, Arnaud Martin, Ali Khenchaf

Laboratoire E^3I^2 (EA 3876)
Ecole Nationale Supérieure des Ingénieurs des Études et Techniques de l'Armement (ENSIETA)
Brest, France
{arnoldan, martinar, khenchal}@ensieta.fr

Abstract: We present a versatile simulator for marine radars that can, in particular, be used in multistatic configurations. Today, most simulators modelize the sea clutter by a random noise; however no obvious relation exists between physical parameters (*e.g.* wind speed or salinity) and the shape of the probabilistic law of noise. On the contrary, we modelize the whole acquisition chain: antennas and their polarization, the shape of the emitted signal, etc. Realistic sea surfaces are generated using the two-scales model on a semi-deterministic basis, so as to be able to incorporate the presence of ship wakes. We present pseudo-raw signals obtained with our simulator. These signals can be further processed and fed to a ship detection and tracking chain. We aim at using this simulation as a tool to benchmark these algorithms and improve them by adding knowledge on the physical uncertainties and the sensor imprecisions.

Keywords: Marine surveillance systems, bistatic radar, bistatic scattering, radar simulation.

I. Introduction

On an average day, more than a hundred and fifty ships transit through the English Channel. Among them, about eight ships carry dangerous goods and could potentially be responsible for ecological disasters similar as the sinking of Amoco Cádiz (1978) or more recently, Erika (1999) and Prestige (2002). Drug smuggling, illegal immigration, or piracy are yet other rampant problems that marine authorities have to face. To improve safety along coasts, especially in zones where intense ship traffic occurs, detection and tracking algorithms for radar-based surveillance systems must be continuously improved. Doing so requires an important insight in the physical phenomena that occur during the acquisition of the data. The problem is that real data with extensive ground truth are barely available today, especially with uncommon, yet promising, configurations such as bistatic radar.

In this paper, we present a simulation tool for marine radars that can be used in multistatic configurations and in various working situations: real aperture or synthetic aperture radars, shore-based or airborne radar. This simulator is intended to help the benchmark of current or future ship detection and tracking algorithms. Today, most radar simulators model the sea clutter by a random noise, such as the Rayleigh or the K-compound law [1]. Knowing that the signal coming from the sea can be modeled as a known noise is a divine gift, because it justifies the use of the much-celebrated Constant False Alarm Rate (CFAR) schemes to distinguish ships from waves when thresholding the return signal [2]. However no obvious relation exists between physical parameters (e.g. wind speed, salinity, etc) and the shape of the probabilistic law of noise. Also, the influence of uncertainties on the motion of the radar vector is seldom modeled. Finally, to the best of our knowledge, all the simulators on the market are designed for monostatic configurations where the transceiver and the transmitter are the same.

To go past these shortcomings, we on the contrary opted to model the whole acquisition chain. We consider among other things the antennas and their polarization, the shape and the frequency of the emitted signal, the influence of the weather on the sea, etc. To determine the sea clutter, realistic sea surfaces are generated using a two-scales model on a semi-deterministic basis. On the largest scale, gravity waves are obtained by synthesizing a random sea according to usual height spectra. Using a ray-tracing technique, the local incidence angles can be determined. Then, the scattering coefficients due to smaller waves (capillary waves), are obtained using a statistical description of the sea on small scales [3]. These coefficients account for the diffusion of the electromagnetic wave due to the roughness of the sea surface. This mixed approach between determinism and statistical description, introduced by [4], allows the user to incorporate the presence of ship wakes on the deterministic part of the sea. Simulating ship wakes is essential as it is a prominent feature in SAR images [5]. The signature of the ship itself could be added by using a database of radar cross sections (RCS) for various typical ships acquired in our anechoic chamber.

Our paper is structured as follows. In section II, we present the simulated bistatic configuration and the bistatic radar equation which is the basis of our simulation. In section III, the physical model of the sea is explained, and three approximate methods are reviewed to compute the scattering matrix from the model of the sea. Section IV explains the main steps of the simulation algorithm. Finally, some first results are presented and commented in the last section.

II. Simulated configuration

The simulated configuration is presented in Fig. 1. It consists of a transmitter X and a receiver R, placed at the

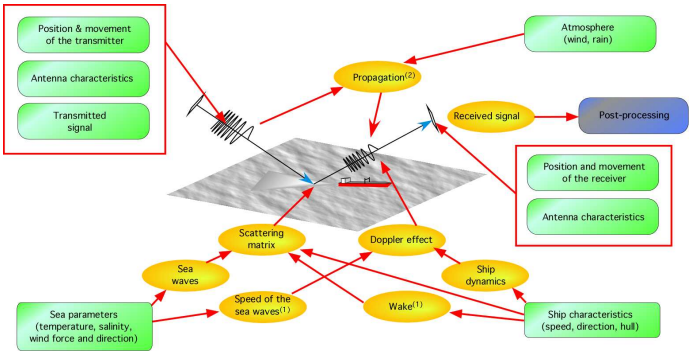

Fig. 1. Simulated configuration. The red arrows indicate the dependencies (some of them are omitted for the sake of brevity). (1): partially simulated; (2) not simulated.

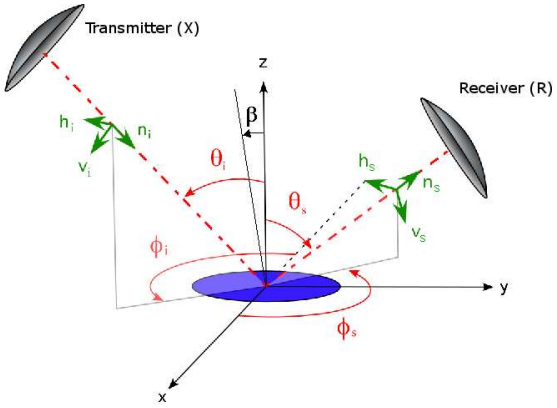

Fig. 2. Bistatic geometric configuration and our notations.

same spatial position (monostatic configuration) or separated (bistatic configuration). The antennas can either belong to a coastal radar, an airborne radar, or a spaceborne radar. Indeed, those will only be a specialization of the more generic radar system that we model here. Such specialization can be achieved either by *i*) tuning variables such as the antenna shape, the carrier frequency or the transmitted signal shape, *ii*) moving the antennas as if they were carried aboard a plane or a satellite and *iii*) using specific post-processing algorithms, such as (eventually bistatic) Synthetic Aperture reconstruction. The target is the sea, which characteristics vary with the wind speed, the salinity, the temperature, and the presence (or absence) of a wake system created by a ship.

We consider the case where the target is located in the far-field of the antenna. Since we are in the far zone, the electric field lives on a plane orthogonal to the direction of propagation. At the vicinity of the target, the incident wave travels in the direction $\hat{\mathbf{n}}_\mathbf{i}$ and the incident electric field $\mathbf{E^i}$ can be described as a 2D vector (E_v^i, E_h^i) in the incident frame $(\hat{\mathbf{v}}_i, \hat{\mathbf{h}}_i)$, such that $\hat{\mathbf{h}}_i \propto \hat{\mathbf{z}} \times \hat{\mathbf{n}}_i$ (as shown in figure 2). Similarly, the electric field $\mathbf{E^s}$ scattered by the target in a given direction $\hat{\mathbf{n}}_s$ can also be described as a 2D vector (E_v^s, E_h^s) in frame $(\hat{\mathbf{v}}_s, \hat{\mathbf{h}}_s)$, with $\hat{\mathbf{h}}_s \propto \hat{\mathbf{z}} \times \hat{\mathbf{n}}_s$. The relation between $\mathbf{E^s}$ and $\mathbf{E^i}$ is described by:

$$\mathbf{E^s} = \mathbf{S}.\mathbf{E^i} \tag{1}$$

where $\mathbf{S} = [S_{mn}]$ is the 2-D scattering matrix. Since the target is, in our case, the sea, only an average of the scattering matrix is known:

$$\langle S_{mn}.S_{mn}^\star \rangle = \frac{\langle E_{mn}^s.E_{mn}^{s\star} \rangle}{E_n^i.E_n^{i\star}} \triangleq \frac{A_0}{4\pi}\sigma_{mn} \tag{2}$$

where A_0 is the surface of the target and indices m, n stand either for the horizontal or the vertical channel. $\mathbf{S}$ depends on the time; techniques for its computation when the target is a rough surface such as sea are presented below. When taking into account the transmitting and the receiving antennas, as well as the travel losses, we can write:

$$r(t) = \frac{e^{-j.k.(r_X+r_R)}}{2\pi.r_X.r_R}.\hat{\mathbf{p}}_R^t \mathbf{G_R}^t.\mathbf{S}.\mathbf{G_X}.\hat{\mathbf{p}}_X.s(t) \tag{3}$$

$s(t)$ is the transmitted signal, $r(t)$ is the received signal, $\hat{\mathbf{p}}_X$, $\hat{\mathbf{p}}_R$ are the polarization vectors of the transmitter and the receiver, k is the electromagnetic wave number and $\mathbf{G_X}$, $\mathbf{G_R}$ are the antenna gain matrices (in amplitude). r_X and r_R are respectively the distance traveled by the electromagnetic wave from the transmitter to the target, and from the target to the receiver. This equation is known as the bistatic polarimetric radar equation and is the basis of our simulation.

When only free-space waves are considered, as we do, the distance $r_X + r_R$ traveled by the wave depends only on the position of the transmitter, the target and the receiver at the time when the signal is emitted, and also on their speed. This is responsible for the well-known Doppler effect. The complete expression of $r_X + r_R$ in the bistatic case may be found in [6]. However, for a more advanced simulation, one should also take into account the fact that the propagation path may not always be linear and that small particles in suspension in the atmosphere may further dampen the signal [7].

III. Obtaining the scattering matrix

Obviously, the most important parameter to know when simulating radar images is the scattering matrix $\mathbf{S}$. In our case, the target is a rough surface, which is usually described using a statistical model. Many methods exist to carry out the computation. This section details three approximate methods to compute this matrix in our case. Note that there are more rigorous methods that exist to carry out such a computation such as the Integral Equation Method, or the Method of Moments but these are unsuitable for fast calculation [8].

A. Physical model of the surface

The scattering properties of the sea depend both on its electromagnetic characteristics and its shape. Sea is generally modelled as a random height field considered as a function of the position (x, y) and the time t. A first-order approximation of the sea surface can be obtained by describing the sea as a linear superposition of individual sinusoidal waves, each having a certain amplitude, pulsation, initial phase, and direction. The shape of the power spectral density (PSD) of the wave height $h(x, y)$ at a fixed time t has been determined

empirically during numerous oceanographic trials. It is a 2D function $\mathcal{S}$, product of two components:

$$\mathcal{S}(K,...) = \frac{1}{K}\mathcal{S}_{1d}(K,...).\mathcal{S}_{dir}(\psi,...) \quad (4)$$

In this equation $\mathbf{K} = [K_x, K_y]$ is the (ocean) wave vector, K is its norm, $\mathcal{S}_{1d}$ is the (1D) omnidirectional wave height spectrum and $\mathcal{S}_{dir}$ is the so-called spread function. The role of the spread function is to describe the fact that waves will tend to be higher as the difference ψ between the direction of the waves and the direction of the wind gets smaller. For example, the Pierson-Moskowitz omnidirectional spectrum can be used [9]:

$$\mathcal{S}_{1d}(||\mathbf{K}||, U_{19.5}) = \frac{a_0}{K^3}\exp\left(-b_0\frac{g^2}{K^2.U_{19.5}^4}\right) \quad (5)$$

where $U_{19.5}$ is the wind speed at an altitude of 19.5 m, g is the acceleration of gravity, $a_0 = 0.0081$ and $b_0 = 0.74$. A great deal of other sea spectra exist, but are generally slight variations on Pierson-Moskowitz, such as the Fung & Lee spectrum [3]. As for the spread function, we followed Longuet-Higgins *et al.* [10] who proposed:

$$\mathcal{S}_{dir}(\psi, s) = \left(\frac{2^{2s-1}}{\pi}\right)\left(\frac{\Gamma^2(s+1)}{\Gamma(2s+1)}\right).\cos^2(\psi/2) \quad (6)$$

where s is the wind-spread parameter, a function of wind speed and frequency. To simplify, and because the choice of s has always been very empirical in the literature, we took $s = 1$ in this paper so that the normalization factor amounts to $4/\pi$. It is interesting to note that many ground structures (fields, etc) can also be modeled using this approach; the computation of the diffusion matrix will be exactly the same except for the fact that the dielectric constants and the spectra will change.

B. Derivating the scattering matrix from the sea spectra

Common approaches include the Kirchoff Approximation (KA) and the Small-Perturbations model (SP). Another method is the Two Scales (TS) method which is a good compromise between the previous two methods, and has been recently extended to the bistatic case by Khenchaf and Airiau [11].

a) The Kirchhoff Approximation: In the KA model, the assumption is made that the curvature of the waves is large enough in front of the electromagnetic wavelength so that they may be locally approximated by a tangent plane; the geometric optic approximation will then be used. This amounts to considering that only specular points on a lighted surface will actually contribute to the received signal. In a far-field configuration, the scattering coefficients will thus be proportional to the probability of finding such specular points, given the configuration of the transmitter and the receiver:

$$\sigma_{mn} = \frac{\pi.k^2||\mathbf{q}||^2}{q_z^4}|U_{mn}|^2\mathrm{Pr}(Z_x, Z_y) \quad (7)$$

where $\mathbf{q} = k.(\mathbf{n_s} - \mathbf{n_i}) = [q_x, q_y, q_z]$, U_{mn} is a polarimetric parameter depending on the configuration angles $(\theta_i, \phi_i, \theta_s, \phi_s)$ and on Fresnel coefficients [12]; and $\mathrm{Pr}(Z_x, Z_y)$ is the probability of finding a slope $Z_x = -q_x/q_z$ and $Z_y = -q_y/q_z$ on the sea surface. The slope probability function has been determined empirically and fitted to an analytical curve by *e.g.* Cox and Munk [13]. The KA model is adequate to compute the average specular component for gravity waves, which satisfy to the large curvature condition. It should be noted that the Kirchhoff approximation is only valid when close to the specular direction ($\pm 20°$); when other directions are chosen, the components of $\mathbf{S}$ will be underrated since the diffuse component is not taken into account.

b) The Small Perturbations Model: The derivation of the Small Perturbations model begins by stating that the total electric field $\mathbf{E}$ can be written as the sum of the incident field, the reflected field (specular and diffuse) and the transmitted field. Then, a boundary condition is introduced; in the case where the surface is a perfect conductor, the condition is that the tangential field is null on the surface. The tangential field can be written as: $\mathbf{E_t} = \mathbf{E} - (\mathbf{E}.\mathbf{n}).\mathbf{n}$ where $\mathbf{n}$ is the local normal. $\mathbf{n}$ is then expressed as an expansion in powers of a small quantity ϵ, like the height of the surface or its slope. This allows to write the reflected and transmitted field as an expansion of individual electromagnetic waves in powers of ϵ. At the order zero, the reflected wave is just the specular component over a flat surface. The Small Perturbations model is usually the development to the first order of the reflected field, thus introducing some diffusion. As ϵ must be small, it is supposed that the typical sea wave height is small compared to the electromagnetic wavelength. It is also assumed that no multiple reflections occur. The mathematical derivation of the model allows to introduce the spectral description of the surface height, which we do know. Finally, in the bistatic case, the components of the diffusion matrix and the intercorrelation coefficients are given by:

$$\sigma_{mn} = 8k^4.\cos^2(\theta_i)\cos^2(\theta_s)|\alpha_{mn}|^2.\mathcal{S}(||\mathbf{k'}||, \angle(\mathbf{k'}, \mathbf{u})) \quad (8)$$

where α_{mn} is a polarimetric coefficient that depends on the bistatic angles and the sea permittivity [14]; and $\mathbf{u}$ the vector defining the wind direction. $\mathbf{k'}$ is defined by:

$$\mathbf{k'} = \begin{bmatrix} k.\sin(\theta_s).\cos(\phi_s - \phi_i) - k.\sin(\theta_i) \\ k.\sin(\theta_s).\sin(\phi_s - \phi_i) \end{bmatrix} \quad (9)$$

c) The Two-Scales model: This model has been introduced a long time ago (see, for instance, [15]) to combine the validity domains of both the Kirchhoff Approximation and the Small Perturbations model, and has been extended to the bistatic case by Khenchaf and Airiau [11]. The TS model postulates that the ocean can be seen as the superposition of two categories of waves: gravity waves with large curvature, and capillary waves, which are smaller. In reality, the transition between large waves and small waves is continuous and this is only a good-enough approximation. The diffusion coefficients are given by computing the average on the slopes of the SP diffusion coefficients, for angles expressed in a local frame.

C. Semi-physical simulation of the sea scattering matrix, using a two-scales deterministic /stochastic sea model

The particularity of both the Kirchhoff Approximation, the Small Perturbation method and the Two Scales method,

is that the bistatic angles are given with reference to the average plane of the sea. Once the configuration is set, a diffusion coefficient obtained for a given set of bistatic angles $(\theta_i, \theta_s, \phi_i, \phi_s)$ is an average over the whole sea surface, of the *real* diffusion coefficient. The average encompasses both gravity and capillary waves. The advantage of such a method, is that one needs not to have or generate a particular sea height map, because the coefficients are known on average.

On the other hand, it is not possible to work with a sea structure where deterministic wave structures appear; for example, wakes, which in their simplest form can be modeled by the simple Kelvin wake structure. For this reason, we chose to use a mixed approach, which has already been used by Cochin *et al.* [4] but for monostatic SAR images only. First, we generate a deterministic wake structure which is superimposed over a particular realization of a sea height map, obtained with the sea spectrum. This will represent an elevation map of $n \times m$ pixels. We sample the elevation so that only coarse structure are represented. Subpixellic structures will be considered as a random, fine scale rough surface. We compute the diffusion coefficients for each point of the surface by computing local bistatic angles with respect to the local normals, which are not necessarily the same everywhere. Depending on the angles, we chose either the coefficients given by the Kirchhoff Approximation if the direction is nearly specular, or the coefficients given by the Small Perturbations model. Following the approach given by Thorsos and Jackson [16], we use an average of the two coefficients:

- for co-polarizations:

$$\sigma_{nn} = (1 - w_1)\sigma_{nn,\ \text{SP}} + w_1 \sigma_{nn,\ \text{K}} \tag{10}$$

- for cross-polarizations:

$$\sigma_{nm} = (1 - w_2)\sigma_{nm,\ \text{SP}} + w_2 \sigma_{nm,\ \text{K}} \tag{11}$$

with:

$$\log_{10} w_1(\beta) = -\left(\frac{\beta}{6\pi}\right)^8$$

$$\log_{10} w_2(\beta) = -\left(\frac{\beta}{20\pi}\right)^{1.5}$$

β is the angle between the local surface normal, and the difference of the incident and scattered wave vector. The shape of the weighting functions has been chosen empirically so as to somewhat minimize abrupt changes of slope at the transition between the two models.

Figure 3 shows the value of the scattering coefficients (in dB), for sea state 3 (temperature 20°C, salinity 35 ppm), by setting $\theta_i = 20°$, $\theta_s = 30°$, $\phi_i = 0°$ and by letting ϕ_s vary. The frequency is 10 GHz (X band). As stated above, it appears that the Kirchhoff approximation underrates diffuse scattering (which occurs for ϕ_s between 20 and 160 degrees), compared to values given by the Small Perturbation method. The interpolation gives better results.

Figure 4 shows how the scattering coefficient varies, for an a fixed incidence angle θ_i, and by letting θ_s and ϕ_s vary (ϕ_i is equal to zero).

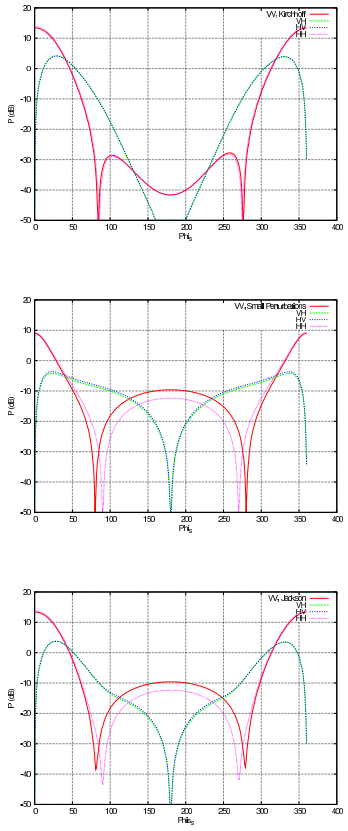

Fig. 3. Scattering coefficients, for $\theta_i = 20°$, $\theta_s = 30°$, $\phi_i = 0°$ and various ϕ_s. $U_{19.5} = 4.53\ m/s$, f=10 GHz. Above: Kirchhoff Approximation, middle: Small Perturbations, bottom: interpolation.

IV. Generation of bistatic radar images

In this section, we describe how we generate the elevation maps, and the processes involved in the creation of the received signal. These operations follow closely the radar equation that has been given at equation 3.

A. Generation of the sea

At the beginning of the simulation ($t = 0$), a random sea is generated using a given sea spectrum, as described at section III-A. As we know the PSD of the sea height map, a random sea for time $t = 0$ can be easily generated by filtering random noise with this PSD. The practical algorithm is the following. First we generate a matrix U of random complex numbers with both real and imaginary parts uniformly distributed between 0 and 1. Then we multiply the square root of the PSD by U, and use an inverse Fourier Transform. c is a normalization factor; its value depends on the implementation of the FFT. With the FFTW package [`www.fftw.org`], for instance, $c = k_{\text{sample}}^g$ where k_{sample} is the sampling step for the spatial wave number of the sea, and g is the dimension of the transform (*e.g.* $g = 2$ for a 2-D sea).

$$z_{t=0}(x, y) = c.\mathcal{F}^{-1}\left(\sqrt{(\mathcal{S})}.U\right)(x, y) \tag{12}$$

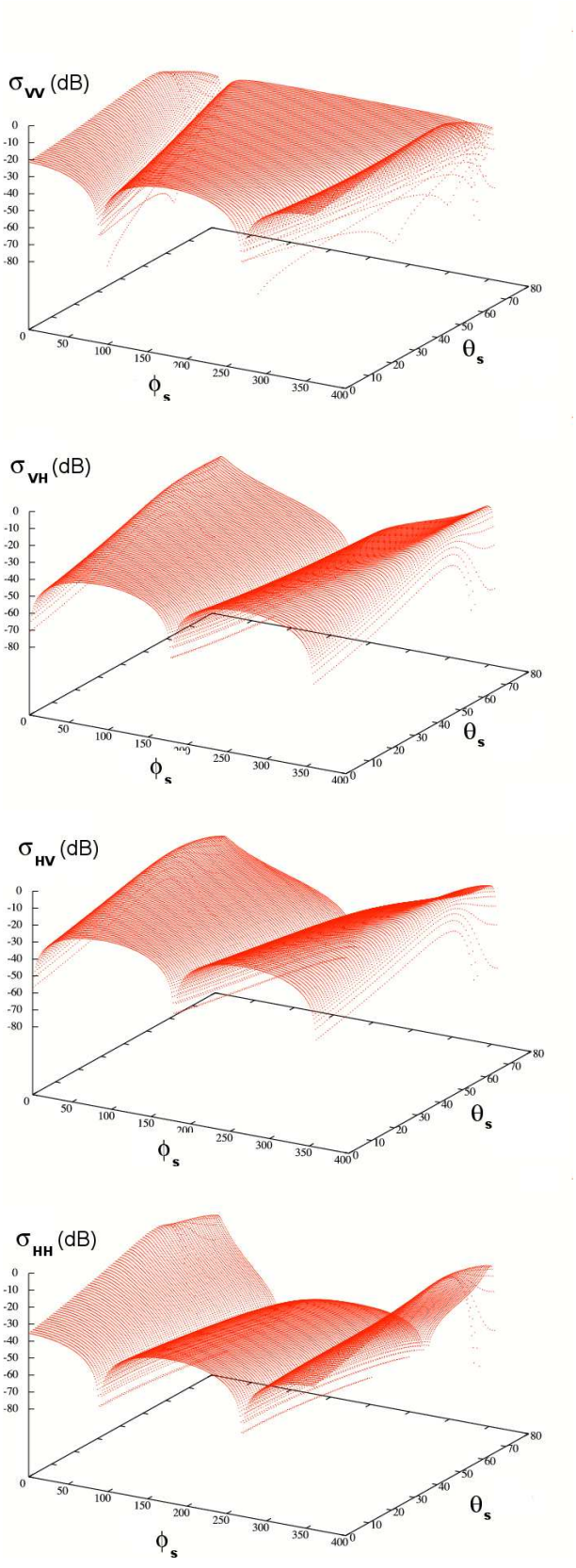

Fig. 4. Scattering coefficients (interpolation between Kirchhoff and Small Perturbations), $\theta_i = 39°$, $\phi_i = 0°$, $U_{19.5} = 4.53\ m/s$, $\psi = 0°$, f=10 GHz.

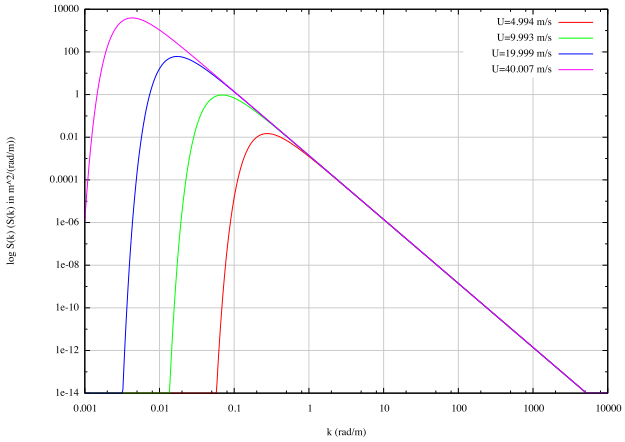

Fig. 5. Pierson-Moskowitz spectrum ($a_0 = 0.0081$), for various wind speeds (at an altitude of 19.5 m).

This method is well known, however the sampling step k_{sample} of the spectrum must be carefully chosen, because the spectrum energy is mostly located in a thin spike located at low spatial frequencies (gravity waves). In order to do this, we noticed that all commonly used sea spectra had their low frequency component following a version of the Pierson-Moskowitz spectrum; and had the form:

$$f(K,U) = \frac{a_0}{K^3} \exp\left(-\frac{b_0}{K^2.U^4}\right) \tag{13}$$

These functions present the following invariant:

$$\forall a, K, U > 0, f(K.a^2, U) = f(K, a.U)/a^6 \tag{14}$$

which means that if the wind changes, the logarithmic bandwidth of the spectrum does not change; if the wind U is multiplied by a the logarithmic curve of the spectrum is merely translated along its $+\infty$ asymptote by a vector $[-2\log a; 6\log a]$. We empirically chose k_{sample} as the quarter of the width of the -3 dB bandwidth; a reference bandwidth has been computed numerically for a given wind speed and all others are deduced using the invariant. The upper wave number was computed using an asymptotic development of the logarithmic spectrum, and taken such as to find a good compromise between the size of the tile to simulate (in pixels), and the typical height of the capillary waves on the pixel. A series of sample Pierson-Moskowitz spectra are plotted on Fig. 5. Notice that when winds become higher, the lower frequency waves augment. Also, we took wind speeds in a geometrical progression of factor $a = 2$; notice that the curves are merely regularly translated, thus illustrating invariant 14.

The sea map at a given date t, can be deduced from the initial sea map by multiplying the Fourier Transform of $z_{t=0}$ by a phase factor $\exp(-j.\omega.t)$. Assuming that the sea depth is d, the temporal pulsation ω of an individual wave is linked to the modulus K of the spatial wave vector by the well-known relation:

$$\omega^2 = g.K.\tanh(d.K) \tag{15}$$

B. Generating the wake

We use a very simple wake model, established by Lord Kelvin to model the perturbations created by a punctual singularity at the surface of a perfect fluid volume, of infinite depth, moving at an uniform speed. This model approximates well the largest waves created by ships when navigating far from the coast. The wave crests and troughs' position are given by the following equation:

$$\begin{cases} x &= A.\cos(\theta).\left(1-\frac{1}{2}.\cos^2(\theta)\right) \\ y &= \frac{A}{2}.\sin(\theta).\cos(\theta) \end{cases} \quad (16)$$

The wake lives in a cone of aperture $38.54°$, where two types of waves can be seen. The transverse waves travel at the same speed V and mostly in the same direction than the ship; they have a wavelength $L_t = 2\pi.V^2/g$. Divergent waves, which form the cone, have a speed $V_d = V.\cos(\theta)$ and a wavelength $L_d = 2\pi.V^2/g.\cos^2(\theta)$. The actual height of the waves is linked to the shape of the hull and the speed of the ship. It should be noted that other phenomena influence the shape of the wake, such as short surface waves induced by the free- surface strain induced by ship-generated internal waves, or turbulent eddies; yet these features are usually best visible in L-band (whereas our application is X-band radar), and therefore have not yet been taken into account.

C. Generating the radar signal

For a given date t, we compute the received signal by performing a series of operations that follow closely the radar equation. First, the position, attitude and speed of the transmitter and the receiver are determined or computed according to the dynamics equation of the carrier. During this step, noise can eventually be introduced in the carrier's dynamics to account for random perturbations of the carrier path. Secondly, we update the sea map, as explained above. Then, for each point at the surface of the sea, we compute *i*) the antenna gains, *ii*) the local bistatic angles, *iii*) the scattering coefficients and finally *iv*) the gain on the horizontal and vertical channel. Also, the time of flight δt_{XT} from the transmitter to the target, and from the target to the receiver (δt_{TR}), is computed with respect to the objects' position and speed at the time when the signal has been emitted, so as to account for the Doppler effect. This allows to add the received signal, written as a delayed version of the emitted signal, in an array representing the received signal as a function of the time and of the distance. To account for the coherent formation of the signal (which yields speckle), the phase of the received signal will be taken as a uniformly random number between 0 and 2π. On the contrary to Cochin *et al.*, we do not work with images at the final SAR resolution, but truly on the raw signal, which enables us to take all phenomena into account (such as antenna gains).

D. Postprocessing

Once the signal is acquired, the signal is fed to a postprocessing stage, which contains the following stages: *i*) adapted range filtering (if the transmitted signal is chirped on a bandwidth Δf; this brings down the range resolution to the theoretical $c_0/(2\Delta f)$, *ii*) beam sharpening (if working on a SAR mode) and *iii*) other miscellaneous processing stages, such as despeckelization.

V. Numerical results

A. Returns in a simple bistatic configuration

In our first simulation (Fig. 6), we generated a sea surface of 64×64 m with the exact same conditions as in Fig. 3. We add a ship cruising with a heading of 35°, having the characteristics of a small motor boat (length of 10 m, beam of 4 m, draft of 1.5 m and speed of 10 kt). The transmitter is located at coordinates $[x = 0, y = 0, z = 256.65]$ (in meters) and the receiver is located at $[x = 32.0, y = 0, z = 87.91]$. The antennas aim at the center of the tile, which yields $\theta_i = 20°$, $\theta_s = 30°$ relatively to the mean sea surface, at the center. The antennas are both rectangular, uniformly illuminated, with a width of 18 cm and a breadth of 14 cm. We plotted in figure 6.a the elevation map and in figure 6.b the modulus of the received signal (when the transmitted signal is of unit amplitude). Figures 6.c to 6.f show the scattering coefficients σ_{mn} (in dB) for each individual scatterer of the sea. This toy example nonetheless shows the clear influence of the bistatic angles since the antennas are close to the surface: each individual point of the surface will be lighted differently and will contribute in a distinct way. Also, notice how the sea scatters the energy even outside of the main antenna lobe, especially for the co-polarized channels.

B. Synthetic Aperture Radar images

We generated various SAR images, with the following setting: we used a canonical rectangular aperture, illuminated uniformly, carried aboard a plane flying at 3,000 m at a distance of 3,000 m from the center of the simulated tile of sea. The antenna aims at the center of the tile. The plane speed is 222 m.s^{-1} (800 km.h^{-1}), the pulse repetition frequency is equal to 222 Hz, hence a pulse is transmitted every meter. The carrier is set to 10 GHz, and the signal is chirped on 75 MHz so as to obtain a range resolution of 2 m (pulse duration: 333 ns); the antenna width is chosen so as to obtain a comparable resolution in azimuth after beamforming. The configuration is here monostatic, so as to be able to reuse existing SAR software; however, bistatic SAR [17] may be readily used as well.

In these experiments, for each transmitted pulse, the reflected signal for each elementary scatterer ("pixel") is computed and the corresponding signal is added to an array representing the temporal raw signal that would be received for the transmitted ping. Between each ping, the sea height map is not recomputed; although it would be very possible, this is a time-consuming process not really justified here because the illumination time is very short, typically below 0.25 s, which means that movement of the waves is negligible. The total computation time for each pulse is of about 12 s (for a 512×512 mesh, with a 3 GHz Pentium IV, the simulation code being written in C). Surprisingly enough, the bulk of the

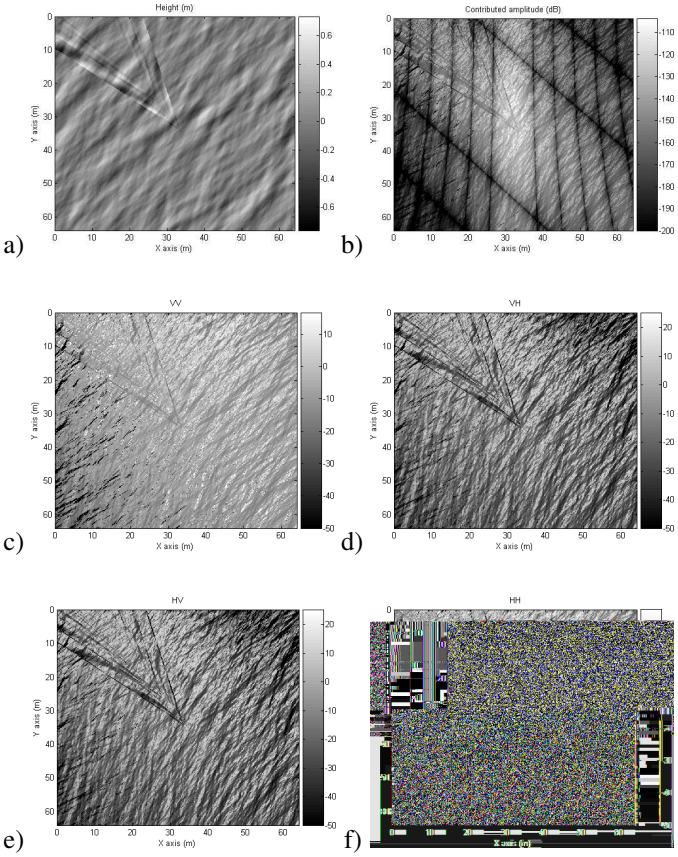

Fig. 6. Simulation 1

computation time is taken by the 10-lines-long loop writing the pulse in the received signal array (despite aggressive optimization), and not that part of the code which computes the radar cross section of a sea element.

In simulation 2 (Fig. 7), we simulate a sea of state 2 (significant wave height: 0.5 m), with a wind direction of 55°. We add the same ship as in simulation 1. We use a mesh of 512×512 pixels to simulate a sea patch of length 128 m. The arms of the wake are clearly visible and are very bright, as compared to the level of the sea. Cross-polarized channels HV and VH offer a better contrast than co-polarized channels, which is usual when observing the sea. The spurious secondary spikes are at least -27 dB below the answer of the wake and are likely due to secondary lobes after range and amplitude compression; in particular, since we took a constant antenna illumination pattern in our example, the secondary (physical) antenna lobes are not tapered off.

In simulation 3 (Fig. 8), we use the same setting, except that the wind direction is 0° (thus blowing in the orthogonal direction to the plane) and the ship has a heading of 45°. The signal to noise ratio between the wake and the sea is lower, which makes sense in the monostatic configuration: when sea waves travel in the look direction, the probability of finding a small element of water reflecting rays towards the transmitter is maximized, which means that the contribution of the sea is more important. Also, we note that the VV channel gives the strongest returns, which is usual when the incidence angle is greater than about 20°. Experiments 2 and 3 show that the visibility of ship wakes is strongly influenced by both the wind direction, the heading of the ship, and the direction of observation; this shows that the observability of ship wakes is by no means guaranteed.

Simulation 4 (Fig. 9) exhibits results that would be obtained when looking at a sea of state 5-6 (the wind speed at 19.5 m is 10 m.s^{-1} *i.e.* about 19.43 kt, with a direction of 30°). The tile has a width of 500 m (512×512 scatterers). The significant wave height of the waves is now of 2.95 m. In those images, the shape of the waves is clearly visible; here again, the cross-polarized channels yield the best contrast whereas the VV channel gives the highest returns.

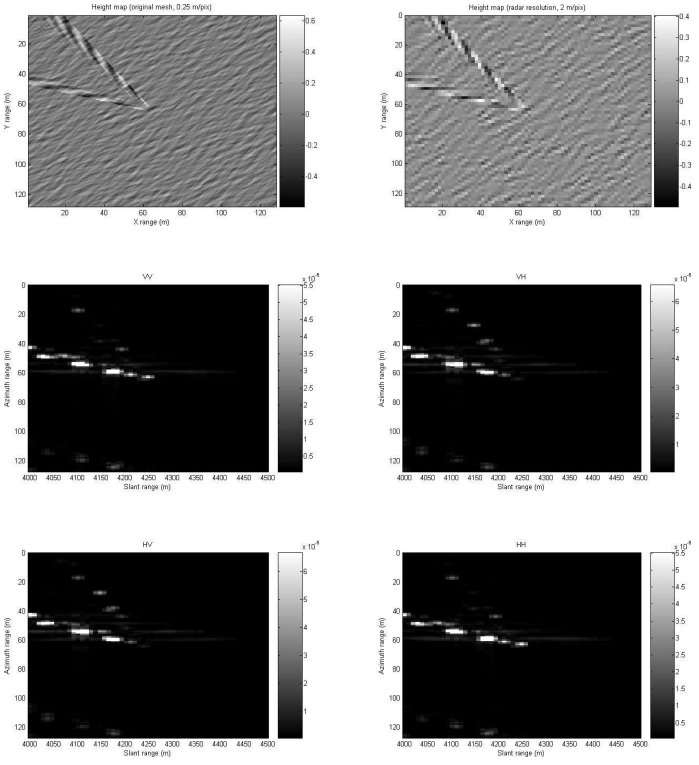

Fig. 7. Simulation 2

VI. Conclusion

We presented a simulator capable of producing pseudo-raw radar signals which can be injected into existing or future post-processing algorithms. This simulator will be used as a tool to generate virtual scenes, so as to test various ship detection and tracking scenarios, using monostatic or bistatic radars. Also, this tool can be used to investigate the influence of natural parameters such as the wind, the orientation of the sensors, on the final images. Indeed, images can be simulated without sensor noise, or, on the other hand, any parameter can be perturbed at will so as to observe the effect on the final image.

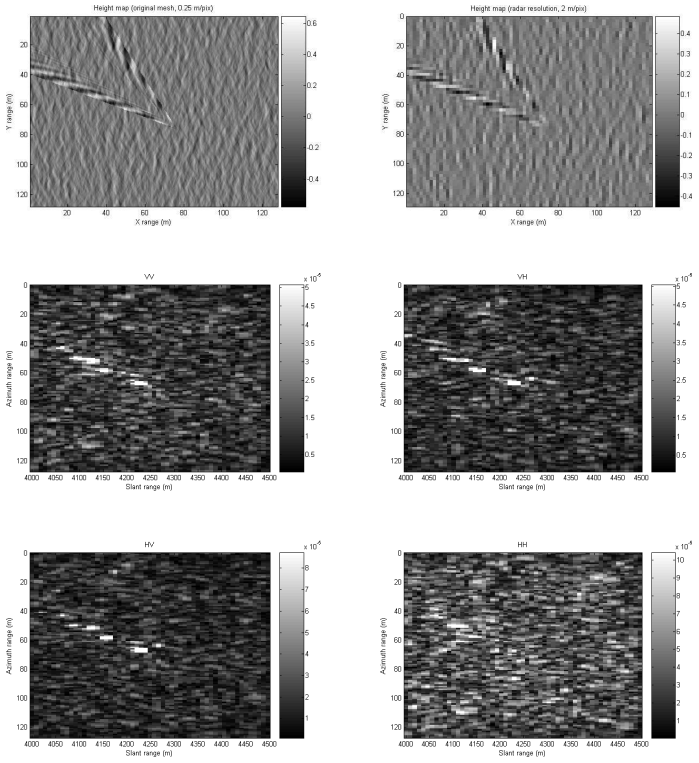

Fig. 8. Simulation 3

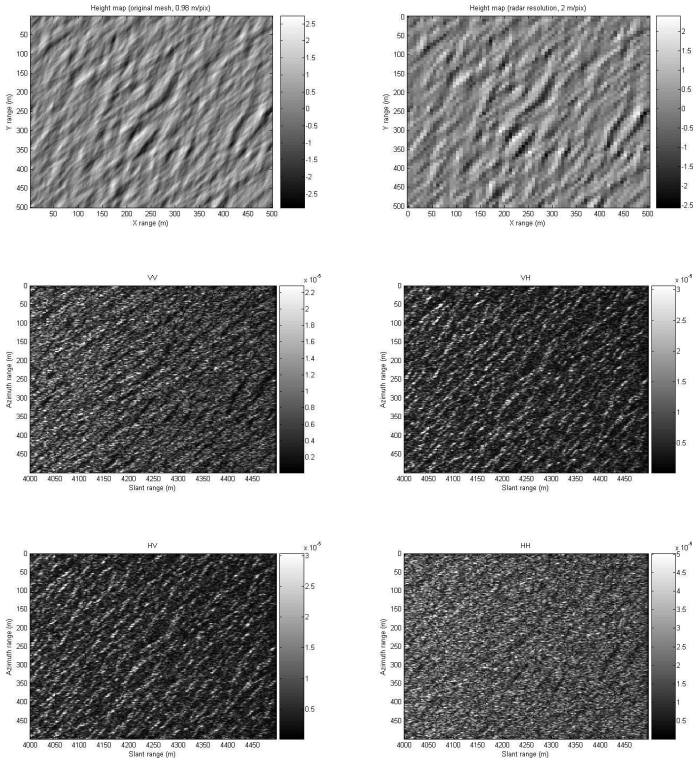

Fig. 9. Simulation 4

REFERENCES

[1] I. Antipov, "Analysis of sea clutter data," Defence Science and Technology Organisation (Department of Defence, Australia), Tech. Rep. DSTO-TR-0647, Mar. 1998.

[2] H. Rohling, "Radar CFAR thresholding in clutter and multiple target situations," *IEEE Transactions on Aerospace and Electronic Systems*, pp. 608–621, July 1983.

[3] A. Fung and K. K. Lee, "A semi-empirical sea-spectrum model for scattering coefficient estimation," *IEEE Journal of Oceanic Engineering*, vol. 7, no. 4, pp. 166–176, 1982.

[4] C. Cochin, T. Landeau, G. Delhommeau, and B. Alessandrini, "Simulator of ocean scenes observed by polarimetric SAR," in *Proceedings of the Comitee on Earth Observation Satellites SAR Workshop*, Toulouse, France, Oct. 1999.

[5] G. Zilman and T. Miloh, "Radar backscatter of a V-like ship wake from a sea surface covered by surfactants," in *Proceedings of the Twenty First Symposium on Naval Hydrodynamics*, Trondheim, Norway, June 1996.

[6] O. Airiau and A. Khenchaf, "A methodology for modelling and simulating target echoes with a moving polarimetric bistatic radar," *Radio Science*, vol. 35, no. 3, pp. 773–782, May-June 2000.

[7] M. I. Skolnik, *Radar Handbook*. New York: McGraw-Hill Publishing Company, 1970.

[8] M. Saillard and A. Sentenac, "Rigorous solutions for electromagnetic scattering from rough surfaces," *Waves in Random Media*, vol. 11, pp. R103–R137, 2001.

[9] M. Tucker and E. Pitt, *Waves in Ocean Engineering*, ser. Elsevier Ocean Engineering Book Series. Elsevier, 2001.

[10] M.S. Longuet-Higgins et al., *Ocean Wave Spectra*. Prentice-Hall, Inc., 1963, ch. Observations of the Directional Spectrum of Sea Waves Using the Motions of a Floating Buoy, pp. 111–136.

[11] A. Khenchaf and O. Airiau, "Bistatic radar moving returns from sea surface," *IEICE Transactions on Electronics*, vol. E83-C, no. 12, Dec. 2000.

[12] F. T. Ulaby, R. K. Moore, and A. K. Fung, *Microwave Remote Sensing: Active and Passive, vol. II*. Artech House, 1986.

[13] C. Cox and W. Munk, "Statistics of the sea surface derived from sun glitter," *Journal of Marine Research*, vol. 13, pp. 198–227, 1954.

[14] A. Ishimaru, *Wave Propagation and Scattering In Random Media (Vol. 2)*. Academic Press, 1978.

[15] G. R. Valenzuela, "Theories for the interactions of electromagnetic and oceanic waves – a review," *Boundary-Layer Meteorology*, vol. 13, no. 61-85, 1978.

[16] E. I. Thorsos and D. M. Jackson, "Studies of scattering theory using numerical methods," *Waves in Random Media*, vol. 1, no. 3, p. S165, July 1991.

[17] F. Comblet, M. Y. Ayari, F. Pellen, and A. Khenchaf, "Bistatic radar imaging system for sea surface target detection," in *Proceedings of the IEEE Conference on Oceans 2005 (Europe)*, Brest, France, June 2005.